Cell Reports

Supplemental Information

Disruption of Transient Serotonin Accumulation by Non-Serotonin-Producing Neurons Impairs Cortical Map Development

Xiaoning Chen, Ran Ye, J. Jay Gargus, Randy D. Blakely, Kostantin Dobrenis, and Ji Ying Sze

Figure S1

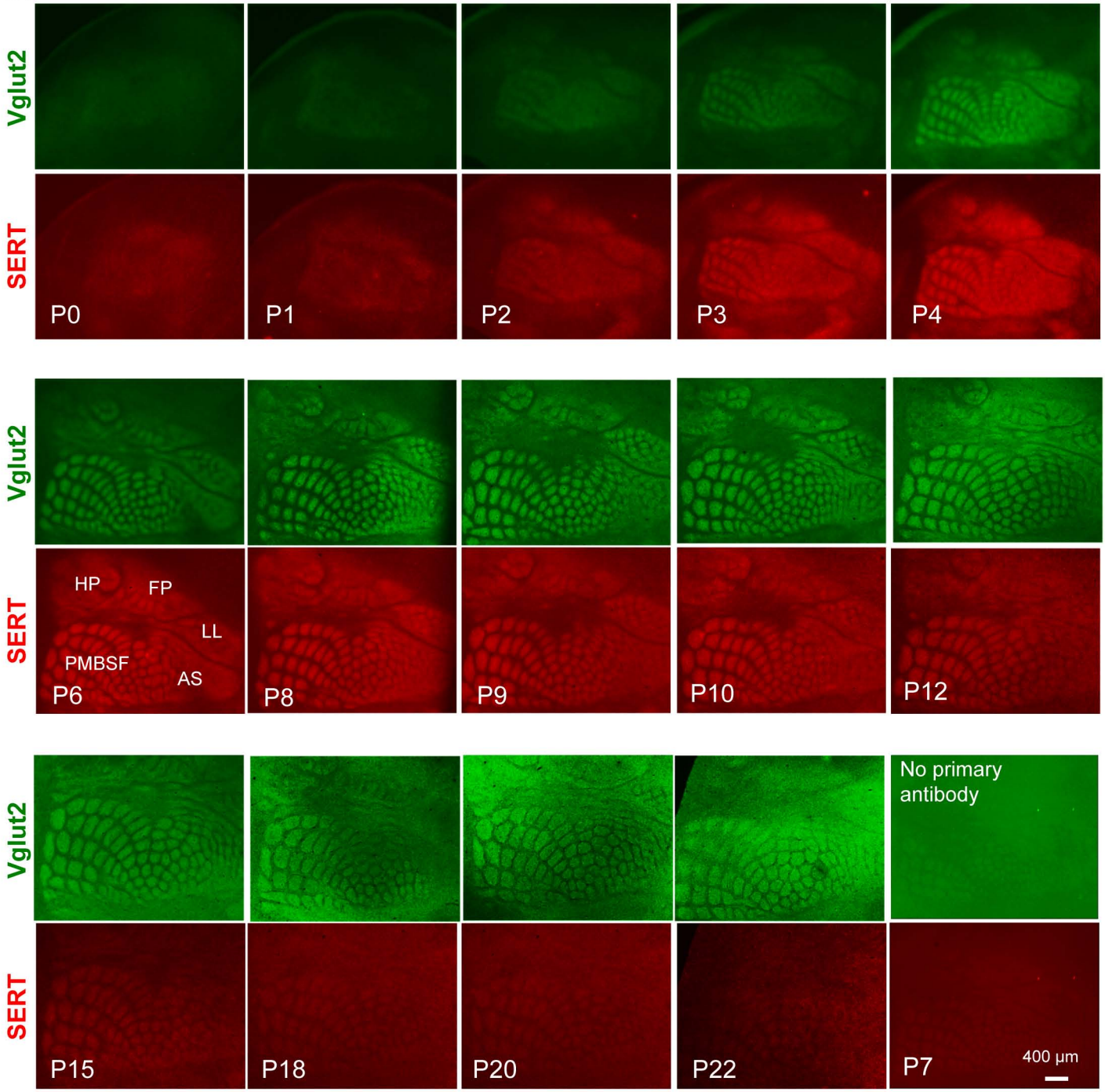
Vglut2
SERT
P0
P1
P2
P3
P4
Vglut2
SERT
HP
FP
LL
PMBSF
AS
P6
P8
P9
P10
P12
Vglut2
SERT
P15
P18
P20
P22
No primary antibody
P7
400 µm

Figure S2

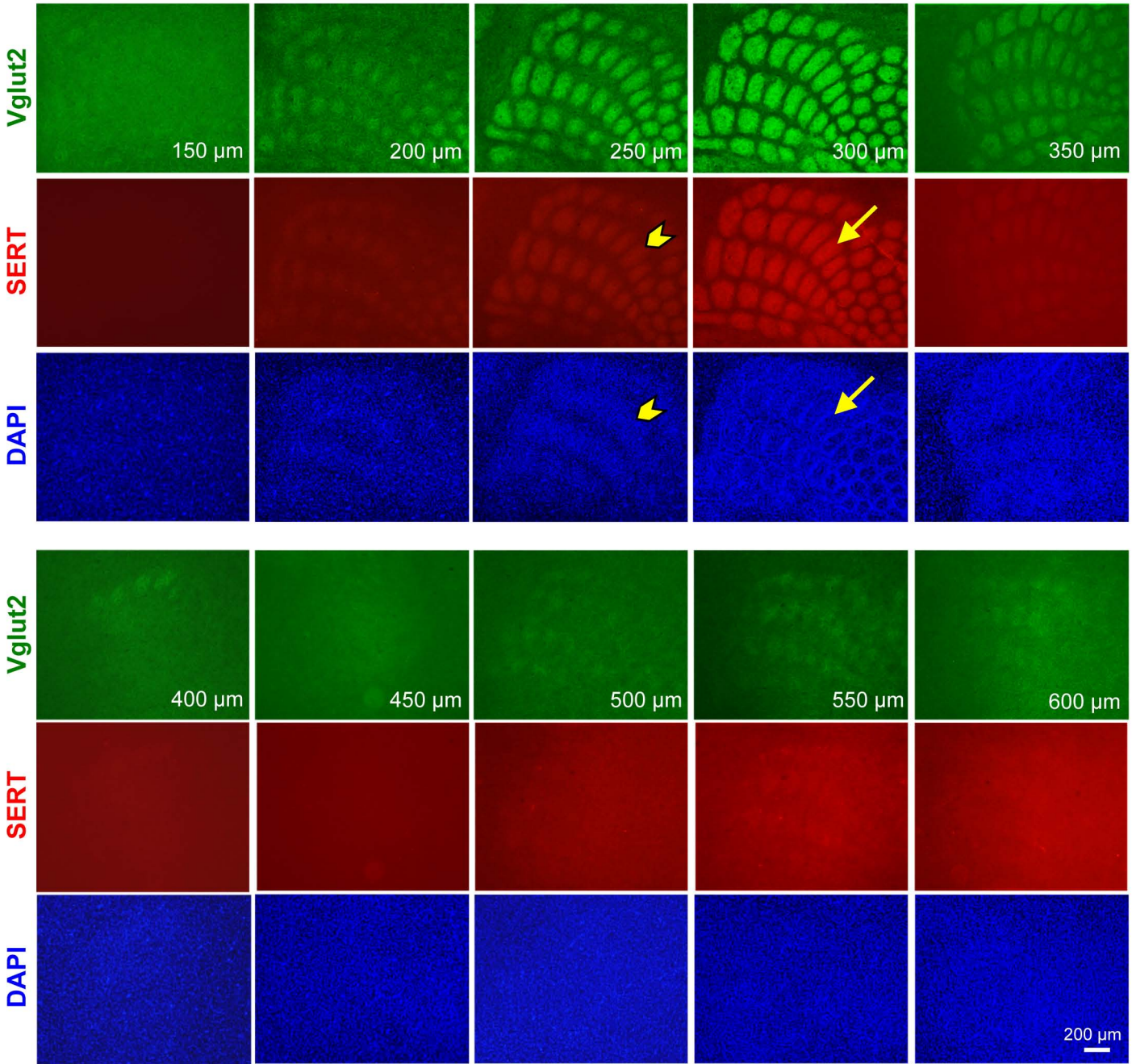
Vglut2
SERT
DAPI
150 µm
200 µm
250 µm
300 µm
350 µm
400 µm
450 µm
500 µm
550 µm
600 µm
200 µm

Figure S3

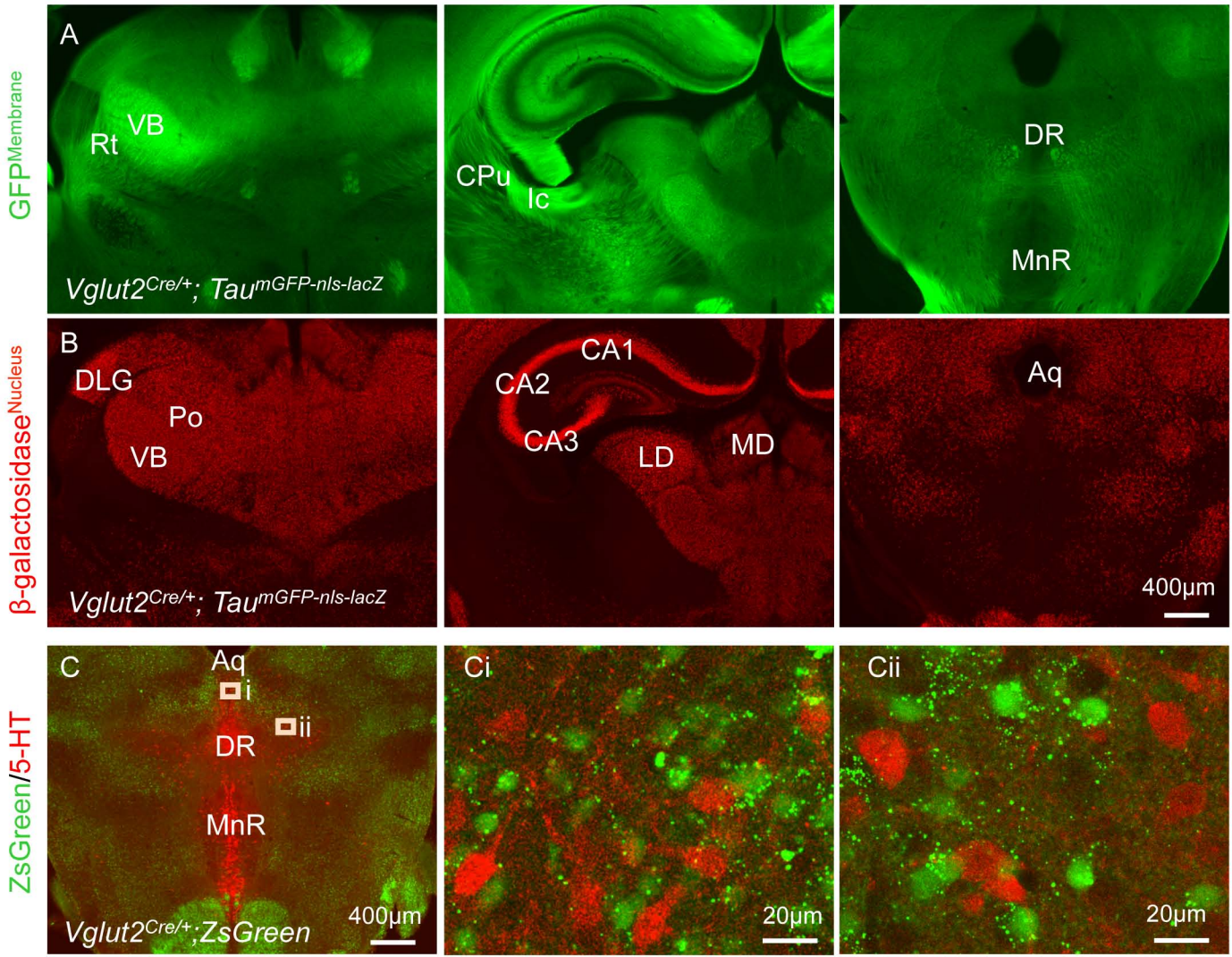
GFPMembrane
A
VB
Rt
CPu
Ic
DR
MnR
Vglut2Cre/+; TaumGFP-nls-lacZ
β-galactosidaseNucleus
B
DLG
Po
VB
CA1
CA2
CA3
LD
MD
Aq
Vglut2Cre/+; TaumGFP-nls-lacZ
400μm
ZsGreen/5-HT
C
Aq
i
ii
DR
MnR
Vglut2Cre/+;ZsGreen
400μm
Ci
20μm
Cii
20μm

Figure S4

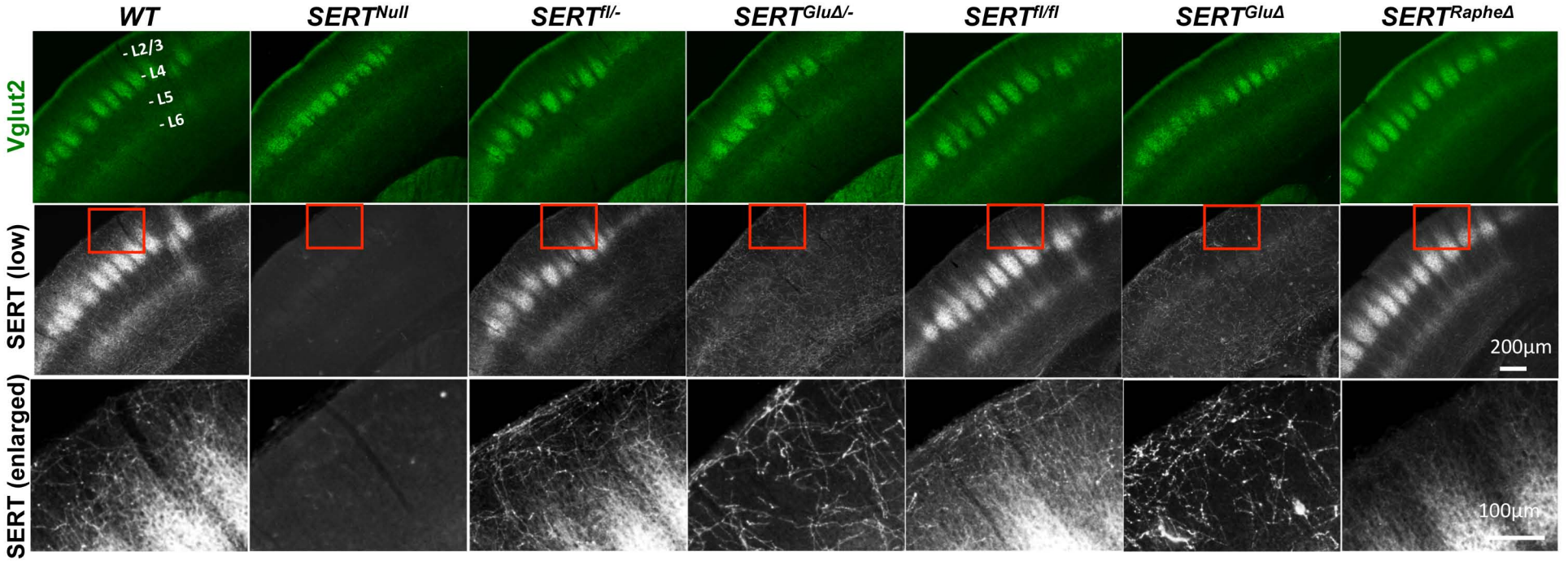
WT
SERTNull
SERTfl/-
SERTGluΔ/-
SERTfl/fl
SERTGluΔ
SERTRapheΔ
Vglut2
- L2/3
- L4
- L5
- L6
SERT (low)
SERT (enlarged)
200µm
100µm

Figure S5

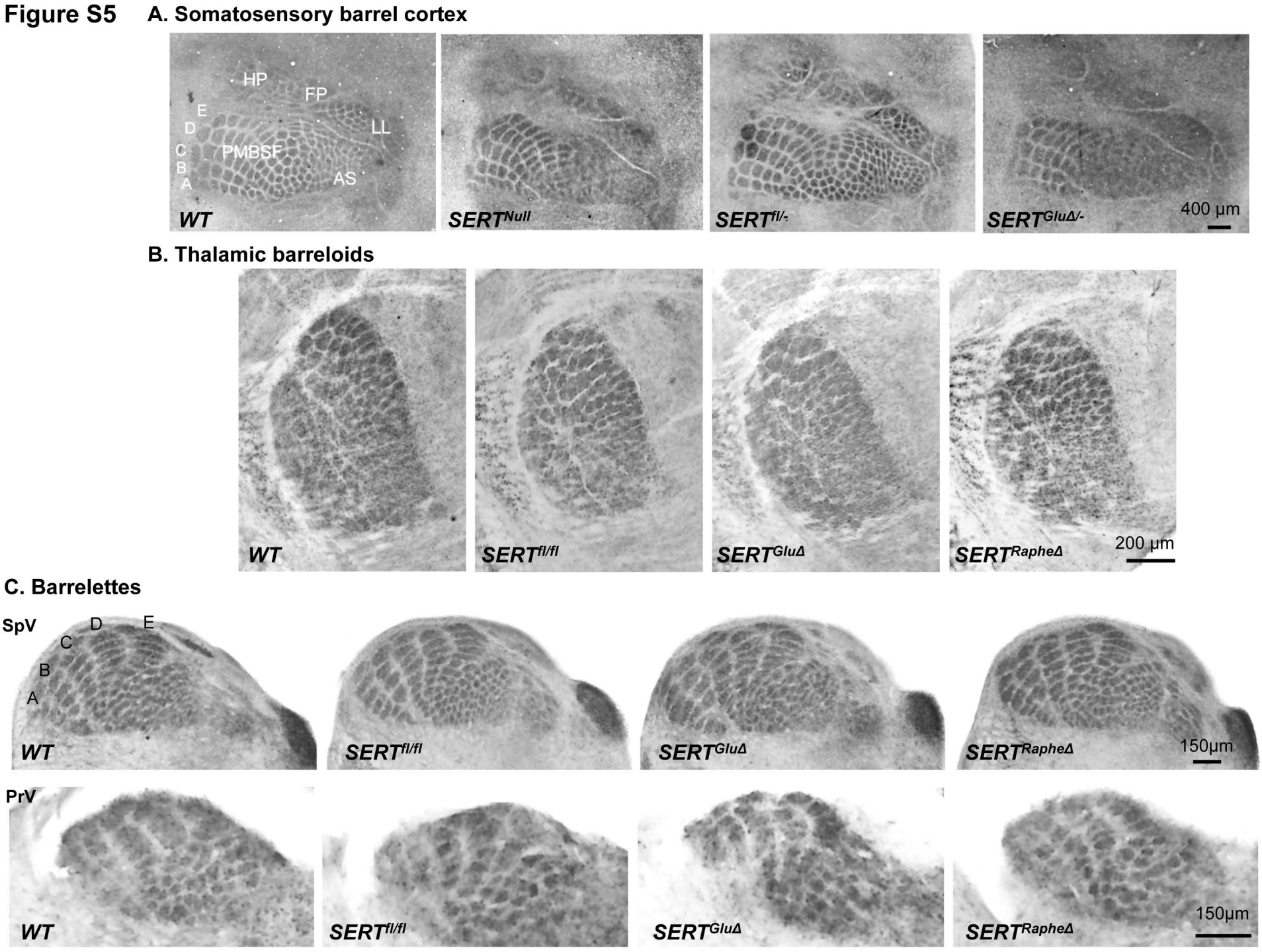
A. Somatosensory barrel cortex
HP
FP
LL
PMBSF
AS
E
D
C
B
A
WT
SERTNull
SERTfl/-
SERTGluΔ/-
400 μm
B. Thalamic barreloids
WT
SERTfl/fl
SERTGluΔ
SERTRapheΔ
200 μm
C. Barrelettes
SpV
D
E
C
B
A
WT
SERTfl/fl
SERTGluΔ
SERTRapheΔ
150μm
PrV
WT
SERTfl/fl
SERTGluΔ
SERTRapheΔ
150μm

Figure S6

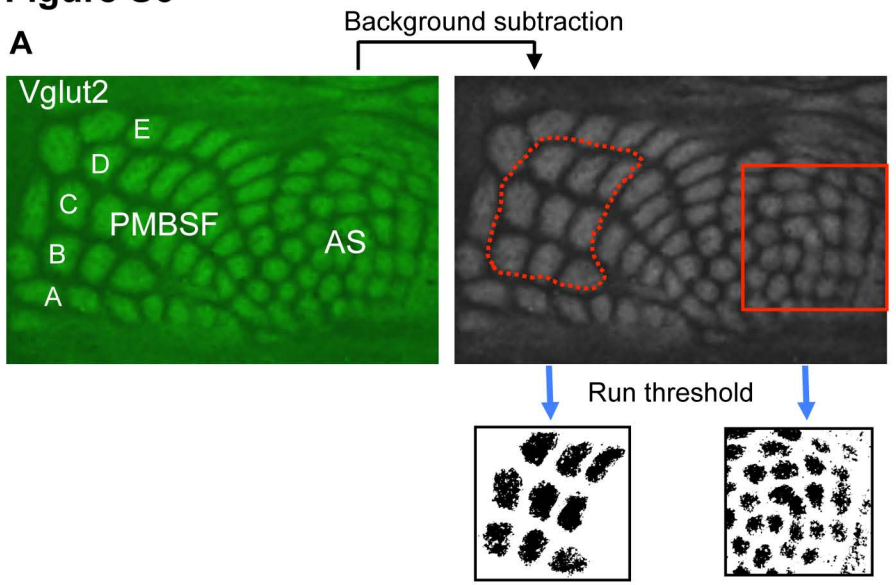

$$\text{BAI-Vglut2} = \frac{\text{pixels with fluorescence signals above threshold}}{\text{Total pixels}}$$

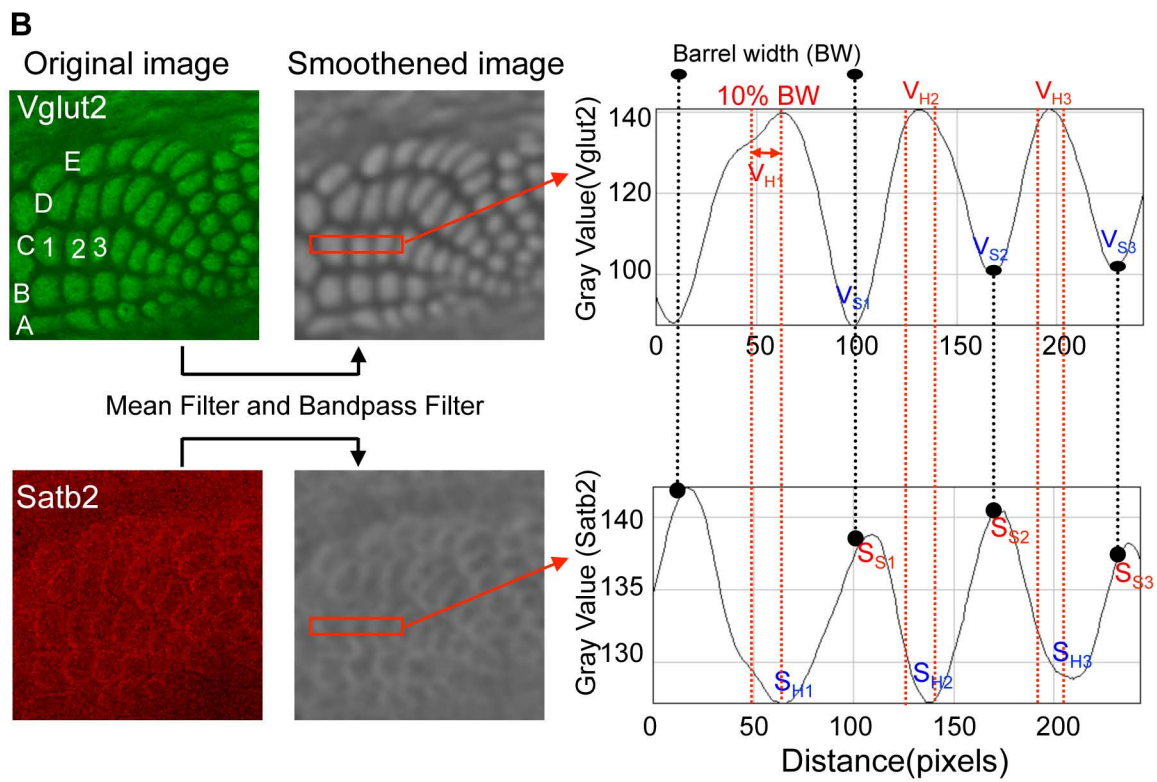

$$\text{BFI-Vglut2} = \frac{(V_{H1}+V_{H2}+V_{H3})/3 - (V_{S1}+V_{S2}+V_{S3})/3}{\text{Mean intensity}}$$

$$\text{BFI-Satb2} = \frac{(S_{S1}+S_{S2}+S_{S3})/3 - (S_{H1}+S_{H2}+S_{H3})/3}{\text{Mean intensity}}$$

Figure S7

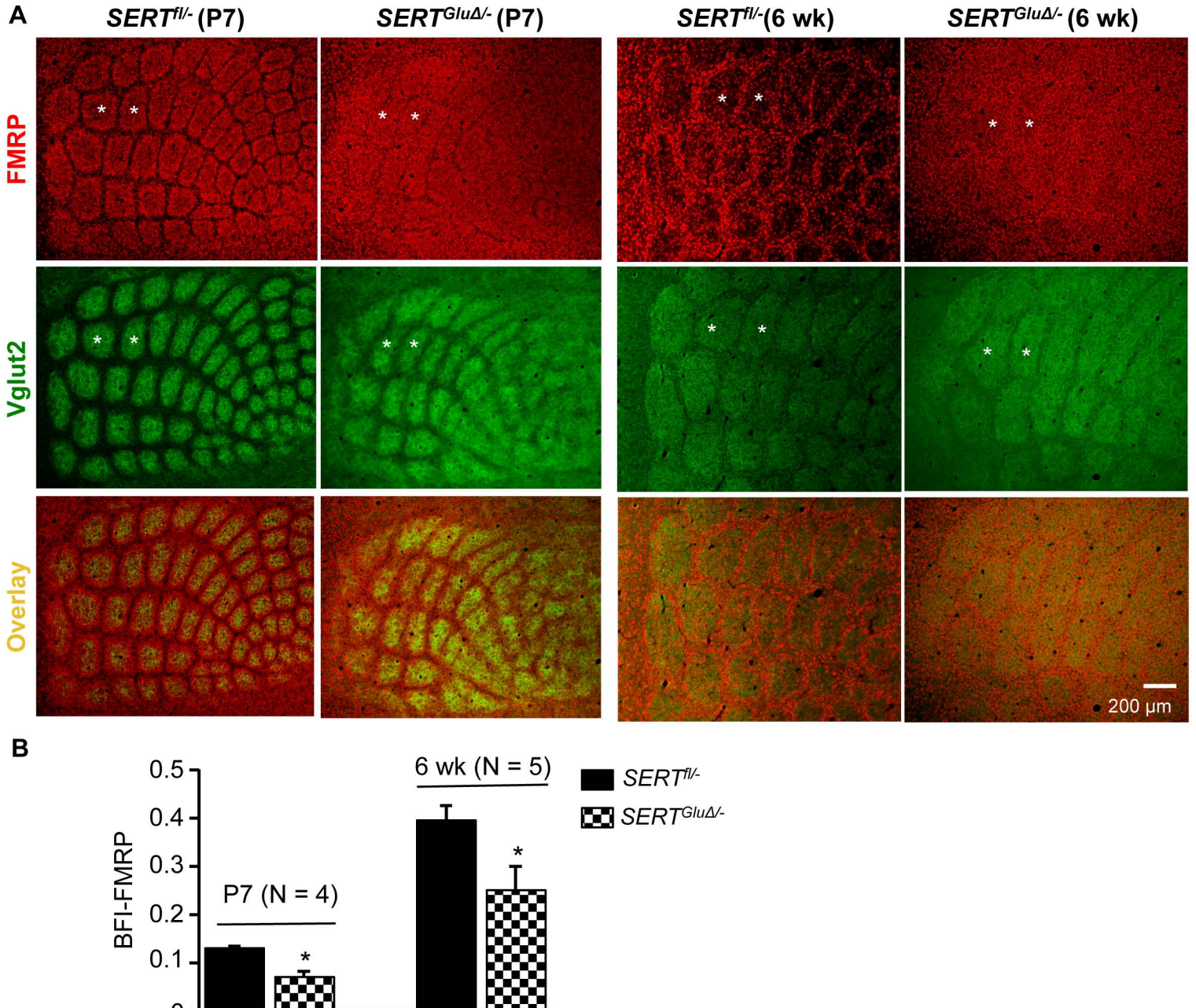
A
SERTfl/- (P7)
SERTGluΔ/- (P7)
SERTfl/- (6 wk)
SERTGluΔ/- (6 wk)
FMRP
Vglut2
Overlay
200 µm
B
BFI-FMRP
0.5
0.4
0.3
0.2
0.1
0
P7 (N = 4)
6 wk (N = 5)
SERTfl/-
SERTGluΔ/-
*

1. Supplementary Figure legends:

Figure S1, Related to Figures 1 and 2. Time course of SERT expression in TCAs projecting to the somatosensory barrel cortex. Double immunostaining of SERT (red) and Vglut2 (green) in tangential sections of WT somatosensory cortex at indicated ages. The rise in SERT immunostaining matched closely with the emergence of Vglut2+ TCA patches in the barrel cortex. SERT immunoreactivity in the TCAs was gradually diminished after P8, and became almost extinguished around P22. SERT staining of TCAs located in the subfields representing whiskers (PMBSF), anterior snout (AS), lower lip (LL), forepaw (FP), and hindpaw (HP) is indicated. The bottom right panels show faint patched background levels of fluorescence in a P7 cortical section processed in parallel without primary antibody. The images represent the results from three independent trials.

Figure S2, related to Figures 1 and 2. SERT immunoreactivity is enriched in Vglut2+ TCA terminal arbors at layer IV of the somatosensory barrel cortex. Typical images of serial tangential sections through the PMBSF of the barrel cortex in P7 control mice double immunolabeled for Vglut2 (green) and SERT (red), with cell nuclei counterstained by DAPI (blue). WT, $SERT^{fl/fl}$ and $SERT^{fl/-}$ mice displayed comparable patterning, and images from a $SERT^{fl/-}$ mouse are presented. The most intense SERT staining co-localized with Vglut2+ TCA patches at layer IV, with each TCA patch surrounded by a ring of densely packed DAPI-labeled cells (arrow). On the top of the barrel structure, SERT+/Vglut2+ TCA patches overlapped with DAPI-labeled cells arranged in stripes (arrowhead), indicating multiple distinct spatial organizations of cortical neurons surrounding SERT-expressed TCAs. Weaker SERT staining also co-localized with Vglut2+ patches in layer VI (3^{rd} and 4^{th} sections in the lower panels). The distance from the pial surface is indicated.

Figure S3, related to Figure 1. *Vglut2-Cre* induced reporter gene expression

A - B. *Vglut2-Cre* is highly active in thalamic VB neurons. Coronal brain sections from P3 mice carrying both $Vglut2^{Cre/+}$ and $Tau^{mGFP\text{-}nls\text{-}lacZ}$ transgenes showed strong Cre-induced expression of membrane-localized GFP (**A, green)** and nucleus-targeted β-galactosidase immunoreactivity (**B, red**) in VB neurons, as well as in several other thalamic nuclei, including dorsal lateral geniculate (DLG) nuclei projecting visual cortex, mediodorsal thalamic nucleus (MD), posterior thalamic nuclei (Po), and medial geniculate nuclei projecting the auditory cortex (not shown). However, some thalamic nuclei, e.g. Reticular thalamic nuclei (Rt) did not display a detectable Cre activity. In addition, *Vglut2-Cre* induced strong reporter gene expression in hippocampal neurons located in CA1, CA2 and CA3 regions. In multiple mice that have been examined, GFP expression and β-galactosidase immunoreactivity were almost absent in the raphe nuclei.

C. *Vglut2-Cre* is not active in raphe 5-HT-producing neurons. 5-HT immunostaining to detect raphe neurons did not co-localize with *Vglut2-Cre*-induced GFP in coronal sections of the brainstem from P3 $Vglut2^{cre/+}$*;ZsGreen* transgenic mice. Ci and Cii are higher magnification confocal images of the areas marked **i** and **ii** in C. Figure 1 shows that *in* $SERT^{Glu\Delta}$ mice the transient SERT expression in the VB and hippocampal neurons was eliminated, whereas SERT expression in raphe neurons unaffected by *Vglut2-Cre*.

Figure S4, relative to Figure 3A. Differential effects of $SERT^{Glu\Delta}$ and $SERT^{Raphe\Delta}$ on SERT expression in the somatosensory cortex. Vglut2 (green) and SERT (grayscale) double immunostaining of coronal sections of P7 somatosensory cortex. WT and control mice showed two distinct classes of SERT+ fibers: fibers that were relatively thin, smooth and co-labeled with

Vglut2+ TCA patches at layer IV (L4) (strongly) and layer VI (L6) (weakly), and fibers that were thicker, punctated, randomly distributed. No SERT staining was discernible in $SERT^{Null}$ mice. In $SERT^{GluΔ}$ and $SERT^{GluΔ/-}$ mice, SERT staining in Vglut2+ TCAs was not detectable, but SERT staining in the thicker fibers remained. In $SERT^{RapheΔ}$ mice, SERT staining in the thicker fibers was dramatically reduced, whereas SERT staining in Vglut2+ TCAs was equivalent to control $SERT^{fl/fl}$ littermates. Images in the third row show an enlarged view of areas outlined by red boxes on images in the second row. Cortical layers are marked.

Figure S5, related to Figure 4A. Knockout of SERT expression in TCAs impairs cortical sensory maps but does not affect lower sensory relay station patterning.

A. Cytochrome oxidase staining of tangential sections through the somatosensory cortex showed defective barrel map architecture in $SERT^{GluΔ/-}$ and $SERT^{Null}$ mice, similar to that seen in SERT KO and $SERT^{GluΔ}$ mice shown in Figure 4A.

B – C. Cytochrome oxidase staining of coronal sections showed comparable patterning of the barreloids in the thalamic VB nuclei (**B**), and barrelettes in the principal sensory (PrV) and spinal (SpV) trigeminal nuclei (**C**) in $SERT^{GluΔ}$ and $SERT^{RapheΔ}$, control $SERT^{fl/fl}$ littermate and WT mice. P7 mutant and control littermate brain slices were stained in parallel, and representative images are shown.

Figure S6, related to Figures 4, 5 and 6. Procedures for quantifying barrel architectures.

A. Quantifying values for barrel appearance index (BAI) of Vglut2 immunohistochemistry in the PMBSF and the subfield corresponding to anterior snout (AS). Tangential sections through the barrel cortex were immunostained for Vglut2, and digital images were processed to determine

the threshold pixel intensity values set at different percentages of the mean pixel value after employing a bandpass filter and minimum value subtraction. The original images were corrected for background using a rolling ball filter and mean value subtraction, and then the "BAI", or the ratio of pixels above different threshold values, determined within the region of interest. For evaluation of PMBSF, an area occupied by nine barrels (rows B to D and arcs 1 to 3) was selected. For evaluation of AS, a 300x300 pixel area next to the PMBSF was selected. Data from 30% threshold are presented.

B. Quantifying values for barrel formation index (BFI) of Vglut2 and Satb2 immunohistochemistry in the PMBSF. Tangential sections through the barrel cortex were double immunostained for Vglut2 and Satb2, and the images of mutant and control littermate samples were taken at a fixed exposure time. After smoothing using the mean filter tool, fluorescence intensities of Vglut2 or Satb2 staining within a rectangle (red box) extended from the C1 to C3 barrels were measured using ImageJ. The horizontal coordinates with minimal values of Vglut2 signals were defined as the positions of septa (S), and the distance between two adjacent septa was defined as barrel width (BW). 10% of the BW located around the horizontal midpoint was defined as the center of barrel hollows (H). Vglut2 and Satb2 signal intensities in individual H and S positions were utilized to calculate BFI values per formulas shown. The same method was utilized for calculating BFI values for FMRP immunostaining of the PMBSF shown in Supplementary Figure S7. The detailed procedures are described in Experimental Methods.

Figure S7, related to Figure 6. Knockout of transient SERT expression in TCAs produces lasting disruption of cortical neuron spatial organization in the barrel cortex.

A. Examining cortical neuron patterning using the fragile X mental retardation 1 protein (FMRP) as a marker. Tangential sections of the PMBSF from *SERT*$^{GluΔ/-}$ and control *SERT*$^{fl/-}$ littermates at P7 and 6 wk of age were double immunolabeled to detect patterning of Vglut2+ TCA patches (green) and FMRP+ cells (red). In control PMBSF, FMRP+ cells displayed a ring structure surrounding Vglut2+ patches at P7, and at 6 wk of age, the Vglut2+ patches appeared to be larger and more spread whereas FMRP+ ring structure became more prominent, showing continuous refinements of the barrel architecture after initial formation. In the PMBSF from *SERT*$^{GluΔ/-}$ mice, the spatial organization of FMRP+ cells was disrupted at P7 and almost completely absent as examined at 6 wk of age.

B. Quantification of FMRP+ cell patterning in the PMBSF using BFI-FMRP (mean ± SEM, *, $p < 0.05$, Student's t-test).

2. Supplementary Experimental Methods:

Immunohistochemistry and histology

Mice were anesthetized by intraperitoneal injection of Avertin (400 mg/kg) prior to transcardial perfusion with phosphate-buffered saline (PBS) followed by 4% paraformaldehyde (PFA) in 0.1 M PB. The brains were removed, post-fixed overnight in 4% PFA, and sectioned in the coronal plane at 40 μm thickness. To obtain tangential sections of the sensory cortices, the neocortical sheets were flattened between two glass slides, post-fixed, and sectioned tangential to the pial surface at 50 μm thickness. Free-floating sections were used for immunostaining with the following antibodies: rabbit α-5-HT (1:50, Dr. W.M. Steinbusch, University of Limburg, the Nethelands), rabbit α-β-galactosidase (1:500, Life Technologies), mouse α-calretinin (1:1000, Millipore), guinea pig α-GABA (1:1000, Millipore), rabbit α-FMRP (1:1000, Abcam), mouse-α-

MAP2 (1:600, Sigma), mouse α-Satb2 (1:1000, Abcam), rabbit α-SERT (1:1000, Millipore), guinea pig α-SERT (1:1000, Frontier Institute, Japan), rabbit α-Vglut2 (1:2000, Synaptic Systems, Germany), and guinea pig α-Vglut2 (1:2000, Millipore). Immunostaining of the proteins and 5-HT was visualized by using Alexa 488 or 568 conjugated secondary antibodies. For detection of GABA immunostaining, biotinylated α-guinea pig IgG and streptavidin-conjugated cy3 (Jackson Immunotechnology) were used. Sections were counterstained with DAPI to detect cell nuclei. Fluorescence images were captured using an Axiocam MR digital camera attached to an AxioImager Z1 miscoscope (Zeiss). Confocal images were collected using Leica SP2 and Zeiss Duo laser scanning confocal microscopes.

For cytochrome oxidase histochemistry, free-floating tangential sections were incubated in a PB (0.1 M, pH7.4) solution containing 0.3 mg/ml cytochrome C in 0.5 mg/ml diaminobenzidine, 40 mg/ml sucrose and 2 μg/ml catalase at 37ºC for 3 hr followed by overnight at 4ºC. Images were captured using a moticam 2300 camera (Motic Inc.) attached to a Leica MS5 microscope.

Cell counts

The distribution of GABA neurons in the barrel cortex was analyzed using GABA immunostaining of serial tangential sections through the PMBSF in P7 mice. Serial confocal images of C2, C3 and C4 barrels were taken at 7 μm intervals using a 20X objective. DAPI was used as a counterstain of cell nuclei for locating barrel boundaries in the PMBSF. We defined barrel walls and hollows using the criteria as previously described (Barnett et al., 2006; Watson et al., 2006). Briefly, a rectangle extended from C2 to C4 was placed in the middle of the barrels, the areas with densely packed DAPI-labeled nuclei between C2 and C3 and that between C3 and C4 were defined as barrel walls, and the area at the midpoint between the two barrel walls as C3

barrel hollow. For each series of confocal images, the number of GABA+ cells in a fixed region of 50 μm x 150 μm on the barrel walls and in the hollow was scored. Segregation of GABA+ cells was evaluated based on the ratio of the GABA+ cell density in barrel walls to that in the hollow. The sections with the highest score for each animal were used for genotype comparison.

Dendrite reconstructions and analysis

Dendrite reconstructions and analysis were performed using similar criteria described previously (Espinosa et al., 2009). Briefly, 60 μm thick tangential sections through the PMBSF of P7 mice were immunostained with antibodies to GABA and calretinin. DAPI was used as a nuclear counterstain for determining barrel boundaries in the PMBSF using a 20X objective. Barrel walls were defined using the same criteria used for GABA cell counts. Calretinin+ cells located close to the edge of barrel walls and co-stained with GABA were randomly selected for quantification. For each neuron, serial confocal images were taken along the Z-axis at 1μm intervals using a 40X objective. To analyze dendritic orientation of GABAergic neurons relative to barrel structures at layer IV, a maximum projection image was created from an image stack, encompassing 18 μm above and below the center of the cell body. This image was superimposed over corresponding lower magnification image to locate the position of the dendrites relative to barrel structures. The dendritic trees were reconstructed using the ImageJ software, and the dendritic paths were confirmed by manually tracing the original confocal images. Following the reconstruction, dendrite length and the number of dendritic branches were quantified using ImageJ software, and branch points were manually counted. To evaluate dendritic orientation, a line crossing the center of the cell body was drawn in parallel to the barrel wall. The barrel housing the majority of dendrite length was considered as the primary barrel, and dendritic profiles leading towards and/or located within the primary barrel were quantified. The same

analysis was performed by reconstruction of calretinin+ GABAergic dendritic trees from Z-stack images collected with an AxioImager Z1 microscope. Results from the two methods are comparable and data from confocal images are presented. Mutants and littermate brain slices were stained in parallel, and 14 – 15 neurons from three mice per genotype group were analyzed.

Quantitative real-time PCR

qPCR was performed to determine relative SERT mRNA levels in the brainstem and VB nuclei from P7 $SERT^{Glu\Delta}$ and $SERT^{Raphe\Delta}$ mice and their $SERT^{fl/fl}$ littermates. *WT* and $SERT^{Null}$ mice were analyzed as additional controls. Brainstem and the VB nuclei of the thalamus were retrieved from P7 mice and RNA from individual brain samples was extracted. 1 μg of RNA from each sample was used for reverse transcription to generate cDNA mix. The cDNA was analyzed by qPCR using the StepOnePlus machine (Applied Biosystems) and SYBR Green detection system (Applied Biosystems). The value of SERT was normalized against the reference gene β-actin, and the average of normalized SERT abundance relative to that of $SERT^{fl/fl}$ samples is presented. The following primers were used:

SERT Fw: 5'-GATTCACCAAGGGGAACGGG-3'

SERT Rv: 5'-TGGTGTAAGGGAGGAGGAAGG-3'

Actin Fw: 5'-GACGGCCAGGTCATCACTAT-3'

Actin Rv: 5'-ATGCCACAGGATTCCATACC-3'

In situ hybridization

In situ hybridization was performed using the IsHyb In Situ Hybridization Kit (Biochain, CA), according to an established protocol (Hendricks et al., 1999) with modifications. SERT RNA probes corresponding to 1510 - 2009 bp of the mouse SERT cDNA as previously reported

(Lebrand et al., 1998) were generated using a DIG RNA labeling kit (Roche, IN). Mice were anesthetized by intraperitoneal injection of Avertin (400 mg/kg) and perfused with 4% paraformaldehyde (PFA). The brains were post-fixed for 2 hr at 4°C, cryoprotected in 30% sucrose, and 25 μm thick frozen sections were used. The sections were treated with 4% PFA for 10 min followed by 11 min 4 μg/ml proteinase K treatment. After acetylation with 0.25% acetic anhydride in 0.1M triethanolamine-HCl buffer and prehybridization, the sections were incubated overnight at 60°C with digoxigenin labeled RNA probes diluted in hybridization buffer. After washing, the sections were incubated with an alkaline phosphatase conjugated anti-digoxigenin antibody and then developed using NBT/BCIP as a substrate. Images of the sections were captured using a Zeiss Axioskop II microscope, and signal intensities of in situ hybridization on the images were quantified using ImageJ software as described (Iwai and Kawasaki, 2009; Toda et al., 2013). Briefly, the dorsal raphe nucleus on individual images was outlined by Freehand Selection tool, and after thresholded at the Mean + 2×SD of the background signal intensity, the signal intensity of the selected region was quantified using the Analyze Particles tool.

Biogenic Amine Measurements

Frozen brain tissues from P7 mice were homogenized in 100 - 750 μl of 0.1M trichloroacetic acid (TCA), 10 mM sodium acetate, 0.1 mM EDTA, 5 ng/ml isoproterenol (as internal standard) and 10.5% methanol (pH 3.8) using an Omni Tissue Homogenizer (Omni International, Kennesaw, GA). Biogenic amine levels were determined by HPLC at the Neurochemistry Core at the Vanderbilt Brain Institute, utilizing an Antec Decade II electrochemical detector (Antec, Boston, MA) operated at 33°C. Twenty μl samples of the supernatant were injected using a Waters 717+ autosampler (Waters, Milford, MA) onto a Phenomenex Nucleosil (5u, 100A) C18 HPLC column (150 x 4.60 mm) (Phenomenex, Torrance,

CA). Samples were eluted with a mobile phase consisting of 89.5% of 0.1 M TCA, 10 mM sodium acetate, 0.1 mM EDTA and 10.5% of methanol (pH 3.8). Solvent was delivered at 0.6 ml/min using a Waters 515 HPLC pump (Waters, Milford, MA). HPLC control and data acquisition were managed by Millennium 32 software (Waters, Milford, MA).

Western Blotting

Following HPLC biogenic amine measurements, tissue protein pellets were solubilized with 200-500 μl RIPA buffer (50 mM Tris, pH 7.4, 150 mM NaCl, 1 mM EDTA, 1% Triton X-100, 1% sodium deoxycholate, 0.1% SDS) containing protease inhibitors (#P8340; Sigma-Aldrich, MO). Protein concentrations were determined by the BCA method (ThermoFisher Scientific, MA). Equal amounts of extracted supernatants were separated by 10% SDS-PAGE, transferred to PVDF membranes, and immunoblotted using SERT (Frontier Institute, Japan; 1:2,000) and β-actin (#A3854; Sigma-Aldrich, MO; 1:10,000) primary antibodies. After washing, membranes were incubated with donkey anti-guinea pig and goat anti-mouse (Jackson ImmunoResearch, PA) secondary antibodies (1:10,000), followed by immunoreactivity detection using chemiluminescence (Western Lightning ECL Pro, MA).

Statistical analysis

Data are presented as mean ± standard error of mean (SEM). The differences between two groups were evaluated by two-tailed, unpaired Student's t-tests. For comparison of multiple groups, one-way ANOVA was performed followed by Bonferroni test. Differences were considered significant when the p value < 0.05.

3. Supplementary References

Barnett, M.W., Watson, R.F., Vitalis, T., Porter, K., Komiyama, N.H., Stoney, P.N., Gillingwater, T.H., Grant, S.G., and Kind, P.C. (2006). Synaptic Ras GTPase activating protein regulates pattern formation in the trigeminal system of mice. J Neurosci *26*, 1355-1365.
Espinosa, J.S., Wheeler, D.G., Tsien, R.W., and Luo, L. (2009). Uncoupling dendrite growth and patterning: single-cell knockout analysis of NMDA receptor 2B. Neuron *62*, 205-217.
Hendricks, T., Francis, N., Fyodorov, D., and Deneris, E.S. (1999). The ETS domain factor Pet-1 is an early and precise marker of central serotonin neurons and interacts with a conserved element in serotonergic genes. J Neurosci *19*, 10348-10356.
Iwai, L., and Kawasaki, H. (2009). Molecular development of the lateral geniculate nucleus in the absence of retinal waves during the time of retinal axon eye-specific segregation. Neuroscience *159*, 1326-1337.
Lebrand, C., Cases, O., Wehrle, R., Blakely, R.D., Edwards, R.H., and Gaspar, P. (1998). Transient developmental expression of monoamine transporters in the rodent forebrain. J Comp Neurol *401*, 506-524.
Toda, T., Homma, D., Tokuoka, H., Hayakawa, I., Sugimoto, Y., Ichinose, H., and Kawasaki, H. (2013). Birth Regulates the Initiation of Sensory Map Formation through Serotonin Signaling. Developmental cell *27*, 32-46.
Watson, R.F., Abdel-Majid, R.M., Barnett, M.W., Willis, B.S., Katsnelson, A., Gillingwater, T.H., McKnight, G.S., Kind, P.C., and Neumann, P.E. (2006). Involvement of protein kinase A in patterning of the mouse somatosensory cortex. J Neurosci *26*, 5393-5401.